



SERS-based Immunoassay on a Plasmonic Syringe Filter for Improved Sampling and Labeling Efficiency of Biomarkers

Journal:	<i>Analyst</i>
Manuscript ID	AN-ART-11-2023-001899
Article Type:	Paper
Date Submitted by the Author:	01-Nov-2023
Complete List of Authors:	Ebbah, Eunice; Illinois State University, Chemistry Amissah, Anthony; Illinois State University, Chemistry Kim, Jun-Hyun; Illinois State University, Chemistry Driskell, Jeremy; Illinois State University, Chemistry

SERS-based Immunoassay on a Plasmonic Syringe Filter for Improved Sampling and Labeling Efficiency of Biomarkers

Eunice Ebbah, Anthony Amissah, Jun-Hyun Kim*, and Jeremy D. Driskell*

Department of Chemistry, Illinois State University, Normal, IL 61790

*corresponding authors: jkim5@ilstu.edu; jdriske@ilstu.edu

ABSTRACT

Rapid, sensitive, and quantitative detection of biomarkers is needed for early diagnosis of disease and surveillance of infectious outbreaks. Here, we exploit a plasmonic syringe filter and surface-enhanced Raman spectroscopy (SERS) in the development of a rapid detection system, using human IgG as a model diagnostic biomarker. The novel assay design facilitates multiple passages of the sample and labeling solution through the detection zone enabling us to investigate and maximize sampling efficiency to the capture substrate. The vertical flow immunoassay process in this study involves the utilization of filter paper embedded with gold nanoparticles (AuNPs) to form a plasmonic substrate. Capture antibody (anti-human IgG) is then immobilized onto the prepared plasmonic paper and inserted into a vertical flow device (syringe filter holder). Sample solution is passed through the filter paper and the target antigen (human IgG) is selectively captured by the immobilized antibody to form an antibody-antigen complex. Next, functionalized AuNPs as extrinsic Raman labels (ERLs) are passed through the filter paper to label the captured biomarker molecules forming a sandwiched geometry. This sandwiched structure enhances plasmonic coupling and SERS signal to provide highly sensitive detection of biomolecules.

1
2
3 Systematic studies to investigate the impact of multiple infuse/withdraw cycles of the sample and
4 labeling solutions reveal that antigen and ERL binding are maximized with 10 and 20 cycles,
5 respectively. The optimized assay achieves a detection limit of ~ 0.2 ng/mL for human IgG with a
6 total assay time of less than 5 minutes, meeting the demands for rapid point of care diagnostics.
7
8 Additionally, the optimized platform was implemented in the quantitative analysis of the SARS-
9
10 CoV-2 nucleocapsid protein, the typical target in commercial, FDA-approved rapid antigen tests
11
12 for COVID-19.
13
14
15
16
17
18
19

20 INTRODUCTION

21
22 The recent SARS-CoV-2 pandemic highlighted the importance of rapid and accurate
23 diagnostic testing that can be widely deployed for large population screening and surveillance.¹
24 Reverse transcriptase polymerase chain reaction (rtPCR) and lateral flow assay (LFA) rapid
25
26 diagnostic tests were primarily employed to surveil patient infection and direct patient isolation;
27
28 however, the slow processing time of rtPCR and poor sensitivity of rapid antigen tests, particularly
29
30 for asymptomatic patients, exposed the need for better point of care (POC) diagnostics.²⁻⁴
31
32 Moreover, rtPCR and lateral flow rapid antigen tests provide limited capacity for multiplexed
33
34 detection. Yet, multiplexed POC tests are highly desirable to identify the causative agent and
35
36 differentiate patients with similar symptoms, such as fever, headache, and congestion and to
37
38 predict disease severity via quantitation of multiple biomarkers.⁵
39
40
41
42
43
44

45
46 Surface-enhance Raman spectroscopy (SERS)-based assays exhibit many of the desirable
47
48 attributes for developing next-generation POC tests.⁶⁻¹⁰ Rationally designed SERS-promoting
49
50 plasmonic architectures have been developed to achieve the requisite sensitivity for clinically
51
52 accurate POC testing. Moreover, SERS spectra are spectroscopically narrow, enabling the
53
54 differentiation of many Raman reporter labels for multiplexed detection, as evidenced in a recent
55
56
57
58
59
60

1
2
3 report that successfully achieved multiplexed detection of 26 labels using SERS.¹¹ Lastly, SERS
4
5 measurements are readily acquired under ambient conditions with commercially available portable
6
7 instruments. Given these known benefits, SERS-based assays have been intensively explored.
8
9 These assays are typically designed in a sandwich format in which the analyte is captured by an
10
11 antibody bound to a solid phase sensing surface. In a second step, a Raman reporter functionalized
12
13 plasmonic particle then labels the bound antigen to facilitate detection and quantitation. Early
14
15 works capitalizing on SERS for readout utilized solid, flat capture substrates that relied on
16
17 diffusion for mass transport, mimicking the sample processing steps of an ELISA.^{7, 8, 12} The
18
19 resulting assays required long incubation times and multiple labor-intensive washing steps,
20
21 limiting utility for rapid diagnostics. Recently, SERS-based assays have been re-imagined to
22
23 address the special requirements of POC testing, using magnetic beads^{13, 14} and LFA formats.¹⁵⁻²¹
24
25
26
27
28

29 LFA s are particularly attractive because the method is well established with validated
30
31 materials, fabrication methods, testing, and precedent for regulatory approval. Extension of LFAs
32
33 to incorporate SERS-labels is straightforward and can be as simple as co-immobilizing a Raman
34
35 reporter molecule on the antibody-gold nanoparticle conjugate extensively used in commercial
36
37 LFAs for visual detection.^{16, 20} Advances in SERS-based LFAs include optimization of the
38
39 plasmonic particle used for labeling to maximize SERS sensitivity or the use of several unique
40
41 labels for multiplexed detection.^{15, 17-19, 21-23} To this end, Zhang *et al.*, developed a highly SERS-
42
43 active core-shell plasmonic nanoparticle for use in a triplexed LFA to detect cardiac biomarkers
44
45 achieving sub-picogram per milliliter LODs.²¹ However, even the advancements in sensitivity and
46
47 multiplexing capacity does not address the inherent limitations in LFA designs, such as low sample
48
49 volume, false negative incurred by the hook effect associated with excess antibodies and/or
50
51 antigens, low multiplexing capacity, and moderate assay times of 5-30 minutes.²⁴⁻²⁶
52
53
54
55
56
57
58
59
60

1
2
3 Ongoing efforts to address some of the limitations of LFAs include the development of
4 vertical flow assays (VFAs).^{24, 27-29} VFAs are emerging as an alternative to LFAs that provide
5 faster results, allow for larger volumes, afford greater multiplexing potential, and circumvent the
6 hook effect.²⁴ Much like LFAs, early VFAs relied on visual readout for detection that limited LOD
7 and clinical accuracy. SERS-detection has been effectively coupled with VFAs to capitalize on the
8 strengths of SERS detection and the VFA format.³⁰⁻³⁴ The concept of a SERS-based VFAs was
9 first introduced and demonstrated by Clarke *et al.*, using a commercially available nitrocellulose
10 vertical flow device and functionalized spherical gold nanoparticles as the SERS tag.³¹ In an effort
11 to improve assay sensitivity, novel plasmonic particles, such as core-shell nanostructures, have
12 been incorporated into VFAs, achieving LODs less than 1 pg/mL.³⁰

13
14
15
16
17
18
19
20
21
22
23
24
25
26
27 Recently, our group reported on plasmonic membranes to facilitate plasmonic coupling for
28 improved LODs, as an alternative approach to anisotropic or core-shell SERS tags.^{34, 35} In that
29 work, we demonstrated that a VFA designed with filter paper embedded with gold nanoparticles
30 rather than the commonly used nitrocellulose yields substantial improvement in SERS signal.³⁴
31 However, much like other LFA protocols, the sample and label made a single pass through the
32 capture membrane. Moreover, the absorbent pad, limited sample, label, and wash volumes to a
33 combined maximum volume of ~350 uL. Here, we use a syringe to facilitate sample and label
34 solutions passage through the capture membrane. The syringe allows for larger sample volumes to
35 be analyzed, as well as multiple cycling steps of the sample and label solutions through the capture
36 substrate to maximize binding efficiency. The capability of the designed filtration device as a
37 SERS-based VFA is established using human IgG as a model antigen. The improvement in
38 sensitivity with multiple sample passages through the capture substrate is clearly demonstrated.

39
40
41
42
43
44
45
46
47
48
49
50
51
52
53
54
55
56
57
58
59
60

1
2
3 After optimizing and assessing the analytical figures of merit, the platform was configured with
4 appropriate matched pair antibodies for the detection of SARS-CoV-2 nucleocapsid protein.
5
6
7
8
9

10 **EXPERIMENTAL**

11 **Materials and Reagents**

12
13
14 Gold nanoparticles (AuNPs) were synthesized using tetrachloroauric (III) acid
15 (HAuCl₄·3H₂O) and citric acid trisodium salt dihydrate from Acros Organics. Extrinsic Raman
16 labels (ERLs) were prepared using unconjugated, citrate-capped AuNP (60 nm) purchased from
17 Ted Pella Inc. Bovine serum albumin lyophilized powder (BSA) and purified IgG from human
18 serum (I4506) were obtained from Sigma-Aldrich. Whatman grade 4 filter paper, phosphate
19 buffered saline, 4-nitrobenzenethiol (NBT), Tween 20, trehalose anhydrous, and polyclonal goat
20 anti-human IgG antibody (31119) were purchased from Thermo Scientific. Humanized
21 monoclonal anti-SARS CoV-2 NP antibody (MBS355887), humanized monoclonal anti-SARS
22 CoV-2 NP antibody (MBS355888), and recombinant SARS CoV-2 nucleocapsid protein (NP)
23 (MBS355894) was purchased from MyBioSource. The syringe apparatus for the assay consisted
24 of three parts purchased from Analytics Shop: male luer adapter to 1/4-28, 1.5 mm bore, PEEK
25 (JR-CMIAPK), Female luer adapter to 1/4-28, 1.5 mm bore, PEEK (JR-CFLAPK), and Union,
26 PEEK, LP 1.3 mm bore, body only, 1/4 -28 (JR-065).
27
28
29
30
31
32
33
34
35
36
37
38
39
40
41
42
43

44 **AuNP Synthesis and Plasmonic Paper Capture Substrate Preparation**

45
46 Highly concentrated spherical AuNPs (60 nm) were synthesized to prepare plasmonic
47 papers. The synthesis of AuNP was achieved using a slightly modified thermal reduction
48 method.³⁶⁻³⁸ Nanopure water (98 mL) was added to a 2.0-mL aliquot of gold solution (1 wt%
49 HAuCl₄·3H₂O) in a 250 mL Erlenmeyer flask with a magnetic stirring bar. The solution was
50 vigorously stirred for 30 min, and the flask was heated to boiling. Trisodium citrate (1.5 mL at 1
51
52
53
54
55
56
57
58
59
60

1
2
3 wt%) was quickly added to the boiling solution and immediately removed from heat. The resulting
4
5 solution was then allowed to stir at room temperature for 40 min, resulting in the formation of
6
7 spherical AuNPs. The final solution was then stored at room temperature without further
8
9 purification prior to use. It is noted that the synthetic conditions readily resulted in the formation
10
11 of a high concentration of AuNPs, allowing for effective fabrication with a filter paper to prepare
12
13 plasmonic substrates in a cost-effective way.
14
15
16

17
18 Whatman grade 4 filter papers with 20-25 μm pore sizes were utilized in the preparation
19
20 of the plasmonic capture substrate. Employing a previously developed dip coating method,³⁹ the
21
22 papers were first dried at 40 °C in an oven overnight and then submerged in 10 mL of the
23
24 synthesized AuNP suspension in a plastic petri dish (60 mm x 15 mm) for 24 h to allow for AuNP
25
26 adsorption. The filter papers were removed from the AuNP suspension, treated with 95% EtOH to
27
28 remove excess AuNPs and dried in the oven (~40 °C) for 30 min. The resulting plasmonic paper
29
30 was then cut into circles of 3 mm diameter using a single-hole punch. To prepare the plasmonic
31
32 capture substrate, 2 μL of 1 mg/mL goat anti-human IgG in a solution of 1% (wt/v) trehalose in
33
34 PBS was applied onto the 3 mm prepared plasmonic paper circles and oven dried for 30 min at 37
35
36 °C. Previously, it has been established that passively adsorbed antibodies bind to AuNPs through
37
38 cysteine residues (e.g., Au-S interactions) to form a robust, irreversibly bound capture antibody
39
40 layer.⁴⁰⁻⁴⁵ The oven dried SERS capture substrates were then blocked with 100 μL , 1% (wt/v) BSA
41
42 solution for 1 h to minimize nonspecific binding before use.
43
44
45
46
47

48 **Extrinsic Raman Label (ERL) Preparation**

49

50
51 Following a previously established procedure, a Raman reporter molecule (4-
52
53 nitrobenzenethiol, NBT) together with a detection antibody were both adsorbed onto commercially
54
55 available 60 nm AuNPs to prepare extrinsic Raman labels (ERLs). Commercially sourced AuNPs
56
57
58
59
60

1
2
3 were used due to high uniformity and stability^{34,46} and the 60 nm diameter was selected because it
4
5 has been reported as the ideal size of Au-based plasmonic NPs for SERS application.^{47, 48} Briefly,
6
7 the pH of a 1.0 mL aliquot of 60 nm AuNPs (Ted Pella, Inc.) was adjusted to pH 8.0 with the
8
9 addition of 50 mM phosphate buffer (40 μ L). A detection antibody (30 μ g) and 1 mM NBT (10
10
11 μ L) were simultaneously added to the AuNP suspension. The suspension was vortexed and
12
13 incubated at room temperature for 90 min to allow maximum adsorption of the antibody and NBT
14
15 onto the AuNPs surface, forming the ERLs. As noted above, antibodies passively bind to form a
16
17 robust layer.⁴⁰⁻⁴⁵ Excess, unbound detection antibody and NBT were removed from the ERL
18
19 suspension via centrifugation at 5000 g for 5 min to pellet the ERL conjugate, removal of the clear
20
21 supernatant, and resuspension in fresh 2 mM phosphate buffer (pH 8.0). Two additional
22
23 centrifugation purification cycles were performed to thoroughly remove unbound antibody and
24
25 reporter molecules. The concentration of ERLs was increased by resuspending the pelleted
26
27 conjugates in half the original AuNP volume of buffer during the final resuspension step of the
28
29 washing cycles for a final ERL concentration of $\sim 5.2 \times 10^{10}$ ERLs/mL. To further block off any
30
31 exposed surface of the AuNPs and mimic physiological ionic strength to prevent protein unfolding,
32
33 10 μ L of 10% (wt/v) BSA and 10 μ L of 10% (wt/v) NaCl were added to the purified ERLs,
34
35 respectively.
36
37
38
39
40
41
42

43 **Syringe Filter Immunoassay Protocol**

44
45

46 The plasmonic capture substrate with pre-immobilized goat anti-human IgG and blocked
47
48 with BSA was placed in a syringe filter apparatus and the fittings screwed to keep the capture
49
50 substrate in place. Sample solutions of antigen ranging in concentration from 0.1 – 200 ng/mL
51
52 human IgG were prepared by dilution of 1 mg/mL human IgG stock solution in PBS. PBS was
53
54 used as a negative control to determine nonspecific binding of ERLs. A 1-mL syringe was loaded
55
56
57
58
59
60

1
2
3 with 100 μL of sample solution containing antigen and passed through the plasmonic capture
4 substrate. Importantly, the sample delivery by the syringe and porous capture substrate allowed
5 for the sample to be passed through the capture substrate by flowing in a forward and reverse
6 direction multiple times to optimize antigen capture efficiency. Next, a 1-mL syringe was loaded
7 with 100 μL of ERLs (2x concentrated relative to stock concentration unless noted otherwise) and
8 passed through the plasmonic capture substrate, again allowing for optimization of the number of
9 passages through the filter to optimize labeling of captured antigen. Lastly, a 100 μL wash buffer
10 (1% wt/v BSA, 5% Tween 20 in PBS) was passed through the filter followed by two additional
11 rinses to remove excess unbound antigens and ERLs, leaving only the specifically bound
12 components on the plasmonic paper. The paper was removed from the filter holder and allowed to
13 dry in a desiccator before SERS analysis. This entire method of analysis, i.e., sampling, labeling,
14 washing, and spectral acquisition, required approximately 5 minutes.
15
16
17
18
19
20
21
22
23
24
25
26
27
28
29
30

31 **Enzyme-Linked Immunosorbent Assay (ELISA)**

32
33
34 An ELISA was performed as a gold standard to compare the analytical performance of the
35 SERS filter assay. To this end, 100 μL of 5 $\mu\text{g}/\text{mL}$ goat anti-human IgG antibody was added to
36 each well of a 96-well Immulon 2HB microtiter plate and incubated overnight at 4 $^{\circ}\text{C}$ to allow for
37 antibody adsorption. The capture antibody solution was removed, each well was rinsed three times
38 with 300 μL of PBS, and the wells were blocked by three sequential additions of 300 μL
39 SuperBlock. Following the third addition/removal of SuperBlock, 100 μL of standard solutions of
40 human IgG prepared in PBS with 1% BSA (0 – 1000 ng/mL) were added to the wells in triplicate
41 and incubated for 2 h. The sample solutions were then removed, each well rinsed three times
42 with 300 μL of PBS containing 1% BSA, and 100 μL of HRP-labelled goat anti-human IgG was added.
43
44
45
46
47
48
49
50
51
52
53
54
55
56
57
58
59
60
The HRP antibody was allowed to react for 2 h before removal and each well rinsed three times

1
2
3 with 300 μL of PBS containing 1% BSA. Finally, 100 μL of 1-step ABTS solution was added to
4
5 each well and the absorbance at 410 nm was recorded on a Varioskan plate reader (Thermo
6
7 Scientific, Inc.) after allowing 20 min for color development of the enzymatic reaction.
8
9

10 11 **Instrumentation**

12
13
14 *UV-Visible Spectrophotometer.* An Agilent 843 spectrophotometer (Agilent Technologies,
15
16 Santa Clara, CA) was used to collect extinction spectra of AuNPs and ERLs. Extinction spectra
17
18 confirmed the successful synthesis of ~ 60 nm diameter AuNPs via assessment of the LSPR band
19
20 position. Furthermore, extinction spectra were compared for unconjugated AuNPs and ERLs to
21
22 confirm the immobilization of the antibody on the ERL. The formation of the plasmonic substrate
23
24 was quantitatively assessed from the difference in the extinction of the AuNP suspension before
25
26 and after loading onto the filter paper. A surface UV-Vis-IR spectrophotometer equipped with a
27
28 reflectance probe (StellarNet) was used to examine the absorption band (350 nm – 1500 nm) of
29
30 the AuNP-loaded plasmonic paper.
31
32
33

34
35 *Dynamic Light Scattering (DLS).* The mean hydrodynamic diameter and size distribution
36
37 of AuNPs and ERLs were measured with a Malvern Zetasizer Nano ZSP. Colloidal suspensions
38
39 were placed in a microvolume disposable Eppendorf cuvette and equilibrated for 60 s at 25 $^{\circ}\text{C}$
40
41 prior to analysis. The reported sizes are the Z-average values calculated from 10 runs, 10 s each.
42
43
44

45 *Scanning Electron Microscopy (SEM).* The distribution of AuNPs across the filter paper
46
47 was examined using a field emission scanning electron microscope (FESEM, Zeiss Sigma 300
48
49 VP) equipped with a Gemini column, capable of operating at low voltages to minimize sample
50
51 damage.
52
53
54
55
56
57
58
59
60

1
2
3 *SERS Analysis.* A ProRaman-L-785B (Enwave Optronics, Inc.) Raman spectrometer was
4 used to acquire SERS spectra. The 785 nm laser excitation source was focused on the sample
5 surface and adjusted to 10 mW. Spectra were collected with a 10 s integration time from random
6 locations on each of the samples. Each sample solution was analyzed on a minimum of two
7 plasmonic papers and three spectra were recorded from each paper. The SERS spectra and
8 intensities were reported as the average of the six spectra collected for each sample. The auto-
9 baseline function built in the Enwave application software (ProRaman Reader V8.2.8) was used
10 to baseline correct each spectrum.
11
12
13
14
15
16
17
18
19
20
21
22
23

24 **RESULTS AND DISCUSSION**

25 *Design and Principle of Filter Assay*

26 **Figure 1A** shows the overview of filtration-based immunoassay, where an antibody is pre-
27 immobilized onto a plasmonic paper to form a robust SERS capture substrate. The plasmonic
28 capture substrate is inserted into the filtration device and flow of sample solution through the
29 porous substrate is achieved using a syringe. The highly specific nature of antibodies and antigens
30 allows targeted analytes in sample solutions to be selectively captured and concentrated by the
31 immobilized antibody on the plasmonic substrate. Next, the addition of ERLs, delivered via
32 syringe, specifically labels the bound antigen, and allows for SERS detection. In our previous
33 work, we established that the AuNPs reliably and uniformly embedded in the capture substrate,^{35,}
34 ⁴⁹ i.e., filter paper, are essential for irreversible adsorption of the capture antibody to the filter
35 support⁴⁰⁻⁴⁵ and yields a sandwiched geometry when ERLs bind to support plasmonic coupling
36 between the AuNPs allowing hotspots to be generated to significantly enhance the SERS signal.^{12,}
37
38
39
40
41
42
43
44
45
46
47
48
49
50
51
52

53 35, 48, 50
54
55
56
57
58
59
60

1
2
3 Previously, a SERS-based vertical flow immunoassay (VFA) was developed in which
4 sample and ERL solutions were sequentially drawn through the plasmonic capture using an
5 absorbent pad.³⁴ The SERS VFA provided rapid and sensitive detection with a non-technical
6 protocol. However, the combined volume of the sample, ERL solution, and rinse buffer was
7 limited to ~350 uL by the absorbance capacity of the VFA plug. Moreover, the sample and ERLs
8 solutions made a single passage through the capture substrate for binding. The syringe filter assay
9 explored in this work has the advantage of using the syringe filter system to potentially improve
10 the binding efficiency of the antigen and ERL and detect much lower concentrations by
11 incorporating multiple forward and reverse passages of sample and label through the capture filter.
12 Additionally, volume of sample, label, and wash solutions that can be passed through the filter
13 paper is theoretically unlimited, unlike VFA and LFAs, to potentially improve sensitivity and
14 further minimize non-specific binding.
15
16
17
18
19
20
21
22
23
24
25
26
27
28
29
30

31 A holder for the plasmonic filter paper was assembled using commercially available
32 components. The filtration device was carefully selected to meet the following criteria: readily
33 assemble/disassemble to accommodate user-selected filter paper, form a tight seal, in-line flow
34 channel above and below the filter to maintain column flow through the filter in both directions,
35 and restrict solution flow to a small, defined area of the filter paper. Plasmonic paper is sandwiched
36 between a male and female threaded luer adapter and held together with a union (**Figure 1B**).
37 Solution is confined to a 1.5 mm diameter flow channel defined by the luer adapters. The threaded
38 fittings provide a tight seal around the plasmonic filter paper and enable easy access to load/unload
39 the filter paper.
40
41
42
43
44
45
46
47
48
49
50
51
52
53
54
55
56
57
58
59
60

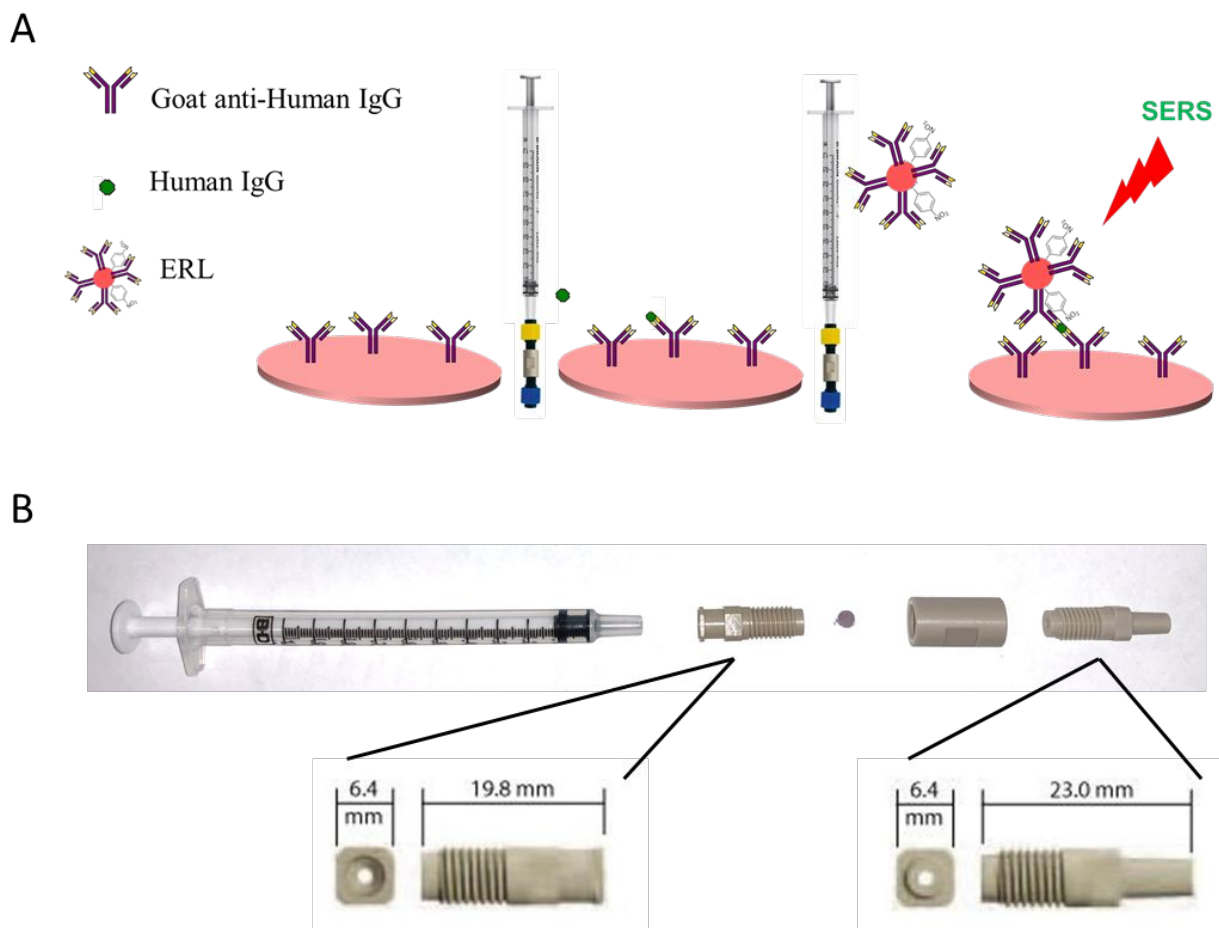


Figure 1. Overview of SERS-based VFIA (A). Photograph of syringe filter apparatus (B).

Feasibility of SERS Filtration Assay

Whatman grade 4 filter paper was selected as the capture substrate support to which AuNPs were embedded.³⁴ The UV-vis extinction spectra of the AuNP suspension before and after the filter paper was submerged for AuNP adsorption are shown in **Figure S1A**. The decrease in color intensity of the AuNP suspension in the cuvette from purple to pink as seen in **Figure S1A** indicates that there has been an effective deposition of AuNPs onto the filter paper to form a plasmonic paper. Additionally, the UV-vis spectra provided semi-quantitative data where the initial concentration of AuNP solution before loading showed a 2.4 extinction at 540 nm while the AuNP solution after loading showed a 0.6 extinction indicating the deposition of AuNP to form

1
2
3 the plasmonic paper. Likewise, the SEM image (**Figure S1B**) also confirms the presence of AuNPs
4 on the filter paper which suggests a successful adsorption of AuNPs on the filter paper. In addition,
5 the surface absorption band was compared to the extinction spectrum of colloidal AuNP solution
6 (**Figure S2**). Unlike well-dispersed colloidal AuNPs in aqueous solution, the surface UV-Vis-near
7 IR spectrum displayed a very broad peak with a gradually declining shoulder line in the entire
8 visible range. This phenomenon has been explained by the presence of small gaps between
9 adjacent plasmonic particles on the substrate to induce interparticle coupling. As randomly
10 aggregated AuNPs are abundantly distributed across filter paper, numerous spacings/gaps between
11 AuNPs readily govern the overall wavelength shift and overlap (i.e., broad band). Although the
12 absorption measurement on a 2-D substrate is challenging due to the measurement conditions
13 involving a strong absorber paper material,^{51, 52} the absorption pattern of the plasmonic paper
14 clearly indicated the presence of a certain degree of locally aggregated AuNPs to induce plasmonic
15 coupling.⁵³⁻⁵⁵

16
17
18
19
20
21
22
23
24
25
26
27
28
29
30
31
32
33
34 Dynamic light scattering (DLS) and UV-vis extinction spectrophotometry were used to
35 characterize the synthesized ERLs. **Figure S3A** shows DLS data where the hydrodynamic
36 diameter of unmodified AuNPs is ~60 nm and that of the ERLs is ~80 nm. The increase in
37 hydrodynamic diameter with the immobilization of the antibody is consistent with the size of an
38 IgG molecule and indicates monolayer formation with no detectable aggregation. UV-vis
39 extinction was also used as a complementary technique to confirm successful formation of ERLs.
40 The unconjugated AuNPs exhibited a maximum extinction at 538 nm (**Figure S3B**). The UV-vis
41 data shows a ~4 nm red shift for the prepared ERLs indicating a change in the refractive index as
42 a result of antibody conjugation to form stable bioconjugates.

1
2
3 Following the successful characterization of ERLs and plasmonic paper, the feasibility of the
4 assay was assessed by performing positive and negative control experiments using the filtration
5 device (**Figure 1**). The plasmonic paper was fabricated with 55 mm diameter filter paper; thus,
6 after forming the plasmonic paper it was cut into 3 mm diameter pieces prior to functionalizing
7 with capture antibody, blocking with BSA, and loading into the filter holder device (**Figure 1B**).
8 As a positive control, 100 μL of a 100 ng/mL human IgG sample in PBS was loaded into a 1-mL
9 syringe and passed through the plasmonic capture substrate. The sample solution was
10 infused/withdrawn 10 times to evaluate the integrity of the filter paper and confirm a tight seal
11 around the capture substrate while confining liquid flow through a defined area of the filter.
12 Following the sampling cycles, 100 μL of ERLs prepared with goat anti-human IgG antibodies
13 were passed through the capture substrate using 10 cycles to label the captured antigen. Lastly,
14 300 μL of wash buffer was passed through the capture substrate using a syringe to remove any
15 non-specifically bound or excess ERLs. The wash buffer was added by cycling 100 μL of solution
16 through the capture filter ten times (infuse/withdraw cycles) using the syringe and repeating two
17 additional times (with fresh 100 μL of wash buffer solution) to thoroughly remove excess unbound
18 ERLs. Upon removal of the capture substrate from the filtration device, it was evident that the
19 solutions were confined to a small area in the center of the filter paper equivalent to the inner
20 diameter of the flow channel of the filter holder. Moreover, visual inspection of the plasmonic
21 paper confirmed that the paper was not damaged as a result of multiple infuse/withdraw cycles of
22 sample, label, and wash solutions. The average of six SERS spectra collected from two
23 independent plasmonic papers used to analyze the positive control is presented in **Figure 2**. As
24 anticipated an intense SERS spectrum was observed with spectral features characteristic of NBT,
25 the Raman reporter molecule used to prepare the ERL. A negative control PBS sample was then
26
27
28
29
30
31
32
33
34
35
36
37
38
39
40
41
42
43
44
45
46
47
48
49
50
51
52
53
54
55
56
57
58
59
60

analyzed by flowing through a capture substrate for 10 cycles, followed by 10 ERL passages, and the same rinsing cycle as the 100 ng/mL hIgG positive control sample. In contrast to the positive control sample, a much smaller intensity was recorded for the negative control. These results establish feasibility of the device to effectively deliver antigen and label to the capture substrate, confirm antigen and ERL are specifically captured and concentrated on the filtration device as a result of antibody-antigen interactions, and non-specific binding of ERLs is minimal.

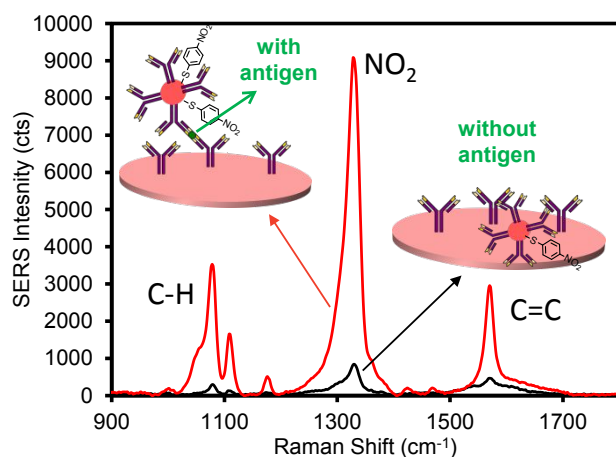


Figure 2. Average SERS spectra for 100 ng/mL human IgG positive control (red) and PBS negative control (black) samples.

Preliminary optimization studies also investigated the use of nitrocellulose as the supporting filter paper. The previous rapid VFA developed by our group used Whatman grade 4 filter paper as an affordable and ideal substrate for making the plasmonic paper.³⁴ However, most commercially available LFIA uses nitrocellulose as a membrane to immobilize capture antibodies because the slightly hydrophobic nature of nitrocellulose allows proteins to bind through hydrophobic interactions.^{56,57} Therefore, we deposited AuNPs onto nitrocellulose membrane (**Figure S4**), and functionalized with goat anti-hIgG as a SERS capture substrates in the VFA. A

1
2
3 100 ng/mL hIgG positive control sample and PBS negative control sample were analyze following
4 the sampling, labeling, and washing procedure used to establish feasibility as described above. The
5 intensity of positive control for the plasmonic capture substrate fabricated with nitrocellulose paper
6 was greater than that of the Whatman grade 4 paper (**Figure S5**). However, the use of nitrocellulose
7 paper resulted in substantially higher non-specific binding of the ERLs in the negative control
8 assay leading to a high SERS intensity as compared to that of the Whatman grade 4 paper (20-25
9 μm), possibly due to the much smaller pore size distribution ($\sim 0.45 \mu\text{m}$).

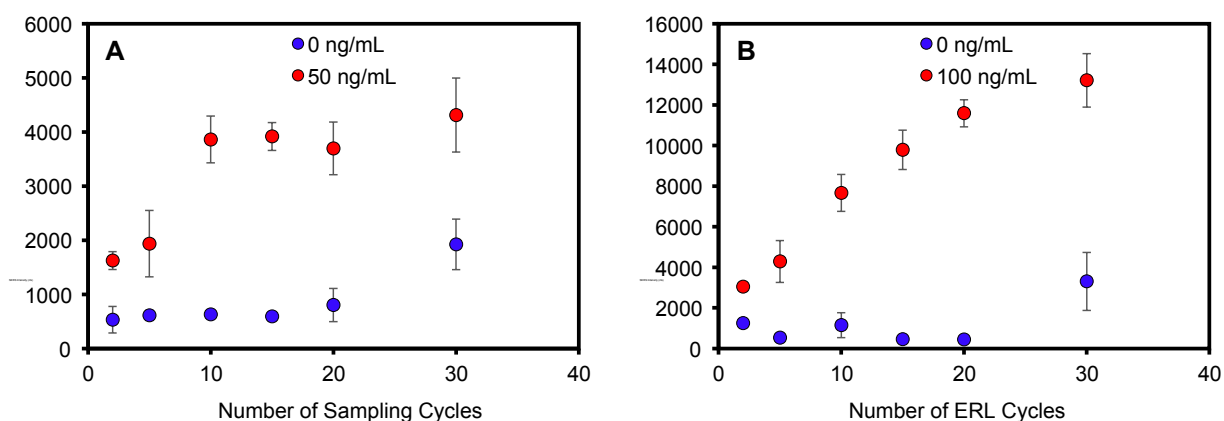
20 21 22 *Effect of Filtration Cycles on Binding Efficiency*

23
24 The primary motivation for developing a filtration-based immunoassay was to enable multiple
25 sampling and labeling cycles to improve binding efficiency. It is well established that actively
26 transporting antigen to an antibody-functionalized capture substrate can reduce the time required
27 for antigen-antibody binding by overcoming binding kinetics limited by diffusional mass
28 transport.⁵⁸⁻⁶¹ However, if mass transport is sufficiently increased, the binding efficiency decreases
29 as the antigen is delivered to the antibody capture substrate at a faster rate than antibody-antigen
30 recognition occurs. For example, the signal due to antigen binding in a filter-based immunoassay
31 decreased as the flow rate increased.⁶² Thus, in previous works, a balance was required to
32 maximize binding, while minimizing assay time, i.e., faster flow rates. In addition, binding is
33 highly flow rate-dependent; thus, flow must be carefully controlled using a syringe pump to
34 achieve acceptable precision and afford quantitative results. Here, multiple passages of sample and
35 labeling solution through the filter using a syringe to infuse/withdraw solutions provide multiple
36 opportunities for interaction to increase the cumulative effective binding efficiency, independent
37 of flow rate, such that binding becomes concentration dependent.

1
2
3 The use of the syringe and the syringe filter apparatus served as an ideal tool to enable multiple
4 passages of sample and/or labeling solutions back and forth through the plasmonic capture
5 substrate. The number of infuse/withdraw cycles of a 100-uL positive control sample consisting
6 of 50 ng/mL hIgG in PBS was varied to investigate the effect of multiple sampling cycles on
7 antigen binding. The ERL labeling step was held constant for each paper at 10 infuse/withdraw
8 cycles and each capture substrate was rinsed with 300 uL of wash buffer. SERS analysis reveals
9 that the antigen binding increases with increasing sampling cycles up to 10 cycles (**Figure 3A**).
10 The binding reaches a maximum at 10 cycles and no additional antigen binding is observed for 15,
11 20, or 30 sample passages through the capture substrate. Moreover, the plasmonic paper substrate
12 maintained visual integrity with the increased number of sampling cycles (Figure S6). A negative
13 control sample was analyzed to determine if multiple passages impacted non-specific binding. The
14 signal for the negative control samples were statistically equivalent up to 20 cycles; however, a
15 slight increase in non-specific binding was consistently observed after 30 sampling cycles.
16
17
18
19
20
21
22
23
24
25
26
27
28
29
30
31
32
33

34 In a similar experiment, positive control hIgG samples (100 ng/mL) and negative control
35 samples (PBS) were cycled through the capture substrate 10 times. The number of ERL solution
36 passages were then varied to investigate multiple labeling cycles on specific and non-specific
37 binding. **Figure 3B** shows that the SERS intensity increased with increased ERL cycles. Unlike
38 the antigen binding step, the signal did not saturate after cycling the ERLs through the capture
39 substrate 30 times. Analysis of the negative samples also show equivalent non-specific binding for
40 less than 20 ERL cycles, but signal for non-specific binding substantially increased with 30 ERL
41 passages. Collectively, these data establish that the optimized assay requires 10 passages of the
42 sample and 20 passages of the ERLs to maximize binding efficiency while minimizing non-
43 specific binding. It is reasonable to expect that more passages of the ERLs are required to
44
45
46
47
48
49
50
51
52
53
54
55
56
57
58
59
60

1
2
3 maximize binding efficiency compared to antigen because the number of antigen molecules are
4 significantly greater than the number of ERLs in the 100 μL volumes – 100 ng/mL antigen is
5 equivalent to 4.0×10^{11} hIgG/mL (670 pM) compared to 5.2×10^{10} ERL/mL (86 pM). Thus, the
6 probability of ERL collision with a target is less than that of the more concentrated antigen,
7 requiring more passages for complete labeling of bound antigen.
8
9
10
11
12
13
14
15
16
17
18



19
20
21
22
23
24
25
26
27
28
29
30
31
32 **Figure 3.** Average SERS intensity of the 1338 cm^{-1} peak as a function of the number of (A)
33 sampling cycles (ERL labeling step was held constant at 10 infuse/withdraw cycles) and (B)
34 ERL cycles (Sampling step was held constant at 10 infuse/withdraw cycles).
35
36
37

38 *Analytical Performance of Optimized Filter Assay*

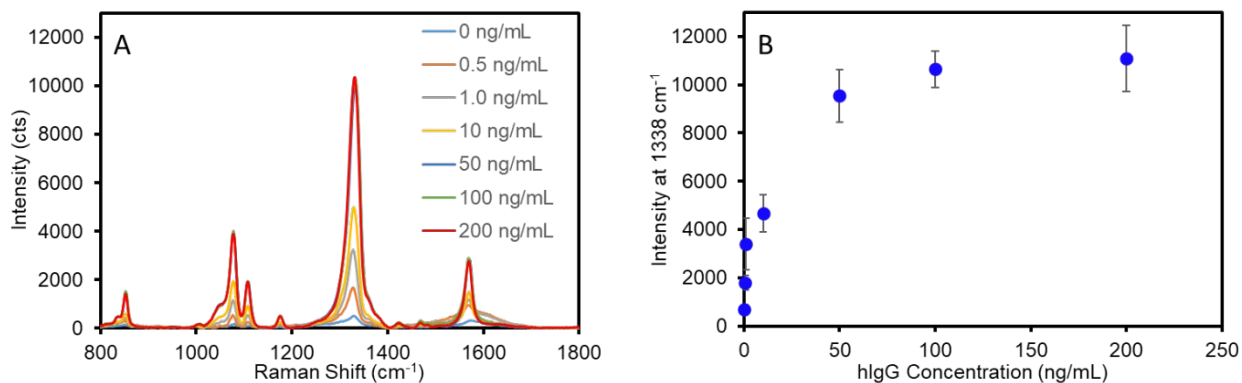
39
40 Standard solutions of human IgG in PBS were analyzed to establish the dose-dependent
41 response and define the analytical figures of merit of the optimized assay. Two independently
42 prepared plasmonic capture substrates and two sets of calibration standards ranging from 0 to 200
43 ng/mL hIgG were analyzed to incorporate inter-assay variability. **Figure 4A** shows the average
44 SERS spectra acquired for each standard concentration. As is evident, the intensity correlates with
45 antigen concentration up to approximately 50 ng/mL, where the signal approaches a maximum
46 value. The concentration-dependent response is plotted in **Figure 4B**. The data clearly
47
48
49
50
51
52
53
54
55
56
57
58
59
60

1
2
3 demonstrated that the optimized assay provides quantitative results and the inter-assay variability
4 in measured signal is ~10-15% for concentrations greater than 1 ng/mL. In addition, the calibration
5 curve shape without any sign of decreasing SERS intensity at high antigen concentrations indicates
6 that this two-step sandwich assay is not limited by the common hook effect.⁶³⁻⁶⁶
7
8
9

10
11
12
13 The detection limit of the assay was determined from the linear best-fit regression analysis of
14 the data for the low concentration range (0-2 ng/mL) (**Figure S7**). Using the best-fit equation for
15 the data in **Figure S7**, the detection limit was calculated as the lowest antigen concentration that
16 would produce a signal equal to that of the mean blank signal plus three times the standard
17 deviation of the blank signal. The optimized assay afforded a detection limit of 0.2 ng/mL (1.3
18 pM) for hIgG. A previously developed SERS-based vertical flow immunoassay for IgG detection
19 achieved a detection limit of 3-8 ng/mL (20-53 pM);³⁴ however, as discussed, the VFA only allows
20 the sample and ERL solution to pass through the plasmonic capture substrate once. Thus, these
21 results suggest that improved sampling efficiency afforded by multiple sampling/labeling passages
22 through the sensing substrate improves the detection limit approximately 20-fold. This detection
23 limit is comparable to those achieved by recently developed SERS-based LFAs for IgG detection
24 that report LODs ranging from 0.1 to 5.0 ng/mL using optimized plasmonic tags.^{22, 23} However, it
25 is important to consider that the antibody binding affinity impacts the assay detection limit and
26 prevents the accurate comparison of inter-laboratory/inter-method LODs in which different
27 antibody-antigen systems are used. To better evaluate the analytical performance of this SERS
28 filtration assay, a sandwich ELISA was conducted using the same antibody-antigen system to
29 allow for appropriate comparison of LODs (**Figure S8**). The ELISA resulted in a detection limit
30 of 1.1 ng/mL, while requiring ~8 h to complete the analysis. This is in contrast to the SERS filter
31
32
33
34
35
36
37
38
39
40
41
42
43
44
45
46
47
48
49
50
51
52
53
54
55
56
57
58
59
60

1
2
3 assay developed in this work that results in a 5-fold improvement in LOD, while significantly
4
5 reducing the assay time.
6
7

8
9 The specificity of the assay was assessed by analyzing relatively simple negative control
10 samples, e.g., PBS and 10% BSA, and a series of serum samples from various species that were
11 diluted 1:100, which represent more complex biological samples. **Figure 5** demonstrates that each
12
13 of the human IgG-negative samples, e.g., PBS, 10% BSA, rabbit serum, bovine serum, and mouse
14
15 serum, resulted in minimal signal. Importantly, the more complex non-human sera samples yielded
16
17 similar signals, i.e., non-specific binding, to the PBS control. In contrast, the human serum sample
18
19 resulted in saturating signal, which is expected considering the concentration of IgG is 5-18 mg/mL
20
21 in undiluted normal human serum corresponding to 50-180 $\mu\text{g/mL}$ in the 100 \times diluted samples
22
23 analyzed here. Collectively, these results confirm the specificity of the SERS filter assay.
24
25
26
27
28
29



44
45
46
47
48
49
50
51
52
53
54
55
56
57
58
59
60

Figure 4. Average SERS spectra ($n = 6$) for hIgG calibration standards (A). Calibration curve for optimized assay (B). Error bars represent the standard deviation for 6 measurements across two independent substrates for each concentration.

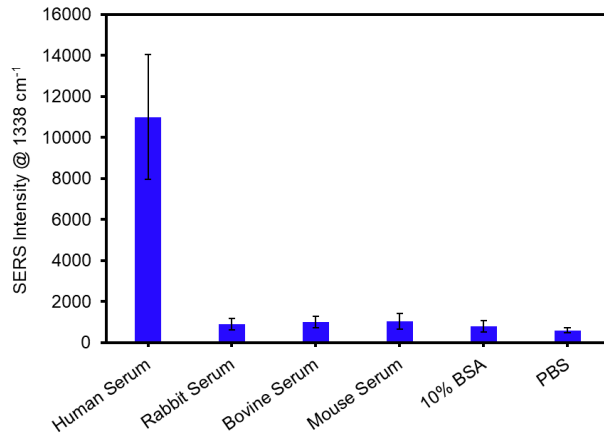


Figure 5. Average SERS intensities for the analysis of sera samples diluted 100-fold with PBS. PBS and 10% BSA were also analyzed as negative control samples. Error bars represent the standard deviation for 6 measurements across two independent substrates for each concentration.

Detection of SARS-CoV-2 Antigen

The assay was re-configured for the detection of SARS-CoV-2 nucleocapsid (N) protein. The N protein is the most common biomarker target of commercial COVID-19 rapid antigen tests. The N protein has a low mutation rate and is antigenically stable among SARS-CoV-2 viral strains for antibody binding,^{1, 67} as evidenced by clinical studies demonstrating that commercial rapid antigen tests (LFAs) targeting the N protein provide equivalent sensitivities for the detection of the Omicron, Delta, and Wuhan-Hu-1 G614 variants.^{67, 68} To this end, the plasmonic paper was functionalized with a humanized monoclonal antibody against N protein and the SERS label was functionalized with a second humanized monoclonal antibody against N protein. The matched pair antibodies were designed to function in a sandwich immunoassay format. Standard solutions of N protein were prepared in PBS and analyzed using the optimized sampling and labeling parameters determined in previous sections. A calibration curve is presented in **Figure 6** and shows a similar concentration-dependent trend observed for the detection of hIgG. A slight increase in non-specific binding for this system, relative to the anti-hIgG model, resulted in an LOD of 1.0 ng/mL (21 pM) for N protein.

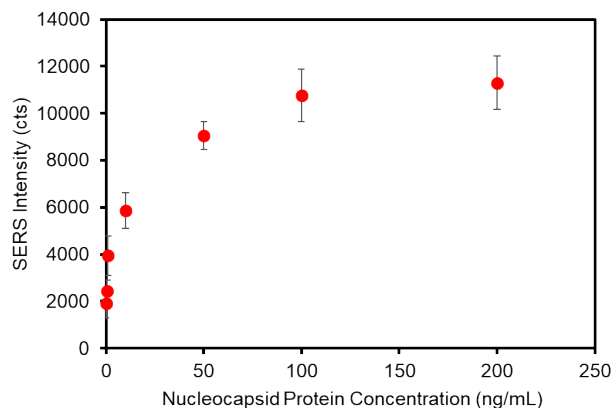


Figure 6. Calibration curve for the detection of SARS-CoV-2 nucleocapsid protein. Each data point represents the average intensity of the 1338 cm^{-1} band collected from 6 different locations on two independently prepared substrates. The standard deviation is represented by the error bars.

CONCLUSIONS

With the aim of developing a novel POC test that is easy to use, rapid, and sensitive, we have designed an optimized SERS-based vertical flow immunoassay that incorporates a syringe filter system to flow the sample and labeling reagent through the detection membrane. This work builds on a previous platform developed in our lab that exploits plasmonic coupling between a nanoparticle-embedded membrane and nanoparticle label to generate exceptionally large SERS enhancements for detection. Here, we explored the use of a syringe filtration device to drive solution through the vertical flow membrane to investigate antigen and label binding efficiency as a function of infuse/withdraw cycles. These results reveal that multiple passages of the sample and ERL suspension through the capture membrane substantially increase antigen-antibody binding efficiency to improve the assay sensitivity with minimal increase in assay time. Current rapid diagnostic platforms such as LFAs and VFAs rely on capillary action to actively transport sample and expedite antigen-antigen binding at the detection zone; however, these platforms limit the number of interactions between the sample and detection zone to a single passage. The data

1
2
3 presented here highlights an opportunity to improve antibody-antigen binding efficiency by
4 implementing multiple, rapid, successive interactions during sampling, and can readily be adapted
5
6 to non-SERS-based vertical flow assays without restraint. Furthermore, successful demonstration
7
8 of specificity for the analysis of a series of serum samples establishes that this platform is capable
9
10 of translation to clinical sample analysis.
11
12
13
14
15
16

17 **CONFLICTS OF INTEREST**

18
19 There are no conflicts to declare.
20
21
22

23 **ACKNOWLEDGEMENTS**

24
25 This work was funded by the National Science Foundation through the Macromolecular,
26
27 Supramolecular and Nanochemistry Program, Award # CHE-2203740. Partial support was also
28
29 provided by Illinois State University. The FESEM multi-user facility was acquired with the
30
31 support from the Division of Material Research (DMR), National Science Foundation (NSF)
32
33 (Award # 2116612).
34
35
36

37 Normal bovine serum was purchased from MyBioSource.

38
39 Normal human serum was purchased from Millipore.
40
41

42 Normal rabbit and mouse serum was purchased from Thermo Scientific.
43
44

45 **REFERENCES**

- 46
47 1. O. Vandenberg, D. Martiny, O. Rochas, A. van Belkum and Z. Kozlakidis, *Nat. Rev. Microbiol.*, 2021,
48 **19**, 171-183.
49 2. S. Lambert-Niclot, A. Cuffel, S. L. Pape, C. Vauloup-Fellous, L. Morand-Joubert, A.-M. Roque-
50 Afonso, J. L. Goff and C. Delaugerre, *J. Clin. Microbiol.*, 2020, **58**, e00977-00920.
51 3. G. C. K. Mak, P. K. C. Cheng, S. S. Y. Lau, K. K. Y. Wong, C. S. Lau, E. T. K. Lam, R. C. W. Chan and D.
52 N. C. Tsang, *J. Clin. Virol.*, 2020, **129**, 104500.
53 4. M. Nagura-Ikeda, K. Imai, S. Tabata, K. Miyoshi, N. Murahara, T. Mizuno, M. Horiuchi, K. Kato, Y.
54 Imoto, M. Iwata, S. Mimura, T. Ito, K. Tamura and Y. Kato, *J. Clin. Microbiol.*, 2020, **58**,
55 10.1128/jcm.01438-01420.
56
57
58
59
60

- 1
 - 2
 - 3
 - 4
 - 5
 - 6
 - 7
 - 8
 - 9
 - 10
 - 11
 - 12
 - 13
 - 14
 - 15
 - 16
 - 17
 - 18
 - 19
 - 20
 - 21
 - 22
 - 23
 - 24
 - 25
 - 26
 - 27
 - 28
 - 29
 - 30
 - 31
 - 32
 - 33
 - 34
 - 35
 - 36
 - 37
 - 38
 - 39
 - 40
 - 41
 - 42
 - 43
 - 44
 - 45
 - 46
 - 47
 - 48
 - 49
 - 50
 - 51
 - 52
 - 53
 - 54
 - 55
 - 56
 - 57
 - 58
 - 59
 - 60
5. R. Lei and C. Mohan, *Crit. Rev. Immunol.*, 2020, **40**, 497-512.
6. Z. Cheng, R. Wang, Y. Xing, L. Zhao, J. Choo and F. Yu, *Analyst*, 2019, **144**, 6533-6540.
7. D. S. Grubisha, R. J. Lipert, H.-Y. Park, J. Driskell and M. D. Porter, *Anal. Chem.*, 2003, **75**, 5936-5943.
8. N. Guarrotxena and G. C. Bazan, *Chem. Commun.*, 2011, **47**, 8784-8786.
9. M. D. Porter, R. J. Lipert, L. M. Siperko, G. Wang and R. Narayanan, *Chem. Soc. Rev.*, 2008, **37**, 1001-1011.
10. J. Langer, D. Jimenez de Aberasturi, J. Aizpurua, R. A. Alvarez-Puebla, B. Auguie, J. J. Baumberg, G. C. Bazan, S. E. J. Bell, A. Boisen, A. G. Brolo, J. Choo, D. Cialla-May, V. Deckert, L. Fabris, K. Faulds, F. J. García de Abajo, R. Goodacre, D. Graham, A. J. Haes, C. L. Haynes, C. Huck, T. Itoh, M. Käll, J. Kneipp, N. A. Kotov, H. Kuang, E. C. Le Ru, H. K. Lee, J.-F. Li, X. Y. Ling, S. A. Maier, T. Mayerhöfer, M. Moskovits, K. Murakoshi, J.-M. Nam, S. Nie, Y. Ozaki, I. Pastoriza-Santos, J. Perez-Juste, J. Popp, A. Pucci, S. Reich, B. Ren, G. C. Schatz, T. Shegai, S. Schlücker, L.-L. Tay, K. G. Thomas, Z.-Q. Tian, R. P. Van Duyne, T. Vo-Dinh, Y. Wang, K. A. Willets, C. Xu, H. Xu, Y. Xu, Y. S. Yamamoto, B. Zhao and L. M. Liz-Marzán, *ACS Nano*, 2020, **14**, 28-117.
11. O. E. Eremina, A. T. Czaja, A. Fernando, A. Aron, D. B. Eremin and C. Zavaleta, *ACS Nano*, 2022, **16**, 10341-10353.
12. J. D. Driskell, R. J. Lipert and M. D. Porter, *J. Phys. Chem. B*, 2006, **110**, 17444-17451.
13. D. Antoine, M. Mohammadi, M. Vitt, J. M. Dickie, S. S. Jyoti, M. A. Tilbury, P. A. Johnson, K. E. Wawrousek and J. G. Wall, *ACS sensors*, 2022, **7**, 866-873.
14. Y. Li, C. Lin, Y. Peng, J. He and Y. Yang, *Sensors and actuators. B, Chemical*, 2022, **365**, 131974.
15. L. Blanco-Covián, V. Montes-García, A. Girard, M. T. Fernández-Abedul, J. Pérez-Juste, I. Pastoriza-Santos, K. Faulds, D. Graham and M. C. Blanco-López, *Nanoscale*, 2017, **9**, 2051-2058.
16. J. Hwang, S. Lee and J. Choo, *Nanoscale*, 2016, **8**, 11418-11425.
17. Z. Rong, R. Xiao, S. Xing, G. Xiong, Z. Yu, L. Wang, X. Jia, K. Wang, Y. Cong and S. Wang, *Analyst*, 2018, **143**, 2115-2121.
18. V. Tran, B. Walkenfort, M. Konig, M. Salehi and S. Schlucker, *Angew. Chem. Int. Ed. Engl.*, 2019, **58**, 442-446.
19. R. Xiao, L. Lu, Z. Rong, C. Wang, Y. Peng, F. Wang, J. Wang, M. Sun, J. Dong, D. Wang, L. Wang, N. Sun and S. Wang, *Biosensors & bioelectronics*, 2020, **168**, 112524.
20. S. Yadav, M. A. Sadique, P. Ranjan, N. Kumar, A. Singhal, A. K. Srivastava and R. Khan, *ACS applied bio materials*, 2021, **4**, 2974-2995.
21. D. Zhang, L. Huang, B. Liu, H. Ni, L. Sun, E. Su, H. Chen, Z. Gu and X. Zhao, *Biosensors & bioelectronics*, 2018, **106**, 204-211.
22. S. Chen, L. Meng, L. Wang, X. Huang, S. Ali, X. Chen, M. Yu, M. Yi, L. Li, L. Yuan, W. Shi and G. Huang, *Sens Actuators B Chem*, 2021, **348**, 130706.
23. H. Liu, E. Dai, R. Xiao, Z. Zhou, M. Zhang, Z. Bai, Y. Shao, K. Qi, J. Tu, C. Wang and S. Wang, *Sens Actuators B Chem*, 2021, **329**, 129196.
24. R. Lei, D. Wang, H. Arain and C. Mohan, *Diagnostics*, 2022, **12**, 1107.
25. Y. Liu, L. Zhan, Z. Qin, J. Sackrison and J. C. Bischof, *ACS Nano*, 2021, **15**, 3593-3611.
26. K. M. Koczula and A. Gallotta, *Essays Biochem.*, 2016, **60**, 111-120.
27. P. Chen, M. Gates-Hollingsworth, S. Pandit, A. Park, D. Montgomery, D. AuCoin, J. Gu and F. Zenhausern, *Talanta*, 2019, **191**, 81-88.
28. Y. K. Oh, H.-A. Joung, S. Kim and M.-G. Kim, *Lab Chip*, 2013, **13**, 768-772.
29. G. M. S. Ross, G. I. Salentijn and M. W. F. Nielen, *Biosensors (Basel)*, 2019, **9**, 143.
30. R. Chen, B. Liu, H. Ni, N. Chang, C. Luan, Q. Ge, J. Dong and X. Zhao, *Analyst*, 2019, **144**, 4051-4059.
31. O. J. R. Clarke, B. L. Goodall, H. P. Hui, N. Vats and C. L. Brosseau, *Anal. Chem.*, 2017, **89**, 1405-1410.

- 1
- 2
- 3
- 4 32. J. H. Granger, A. Skuratovsky, M. D. Porter, Courtney L. Scaife, J. E. Shea, Q. Li and S. Wang, *Anal. Meth.*, 2017, **9**, 4641-4646.
- 5
- 6 33. D. Zhang, L. Huang, B. Liu, Q. Ge, J. Dong and X. Zhao, *Microchim. Acta*, 2019, **186**, 699.
- 7 34. R. Frimpong, W. Jang, J.-H. Kim and J. D. Driskell, *Talanta*, 2021, **223**, 121739.
- 8 35. J. A. Lartey, J. P. Harms, R. Frimpong, C. C. Mulligan, J. D. Driskell and J.-H. Kim, *RSC Adv.*, 2019, **9**, 32535-32543.
- 9
- 10 36. J. Kimling, M. Maier, B. Okenve, V. Kotaidis, H. Ballot and A. Plech, *J. Phys. Chem. B*, 2006, **110**, 15700-15707.
- 11
- 12 37. J. Turkevich, P. C. Stevenson and J. Hillier, *Discuss. Faraday Soc.*, 1951, **11**, 55-75.
- 13 38. M. Wuitschick, A. Birnbaum, S. Witte, M. Sztucki, U. Vainio, N. Pinna, K. Rademann, F. Emmerling, R. Kraehnert and J. Polte, *ACS Nano*, 2015, **9**, 7052-7071.
- 14
- 15 39. J. Magura, A. Zeleňáková, V. Zeleňák and M. Kaňuchová, *Appl. Surf. Sci.*, 2014, **315**, 392-399.
- 16 40. O. Awotunde, S. Okyem, R. Chikoti and J. D. Driskell, *Langmuir*, 2020, **36**, 9241-9249.
- 17 41. H. de Puig, I. Bosch, M. Carré-Camps and K. Hamad-Schifferli, *Bioconjugate Chem.*, 2017, **28**, 230-238.
- 18
- 19
- 20 42. S. L. Filbrun and J. D. Driskell, *Analyst*, 2016, **141**, 3851-3857.
- 21 43. G. Ruiz, N. Ryan, K. Rutschke, O. Awotunde and J. D. Driskell, *Langmuir*, 2019, **35**, 10601-10609.
- 22 44. K. Siriwardana, A. Wang, K. Vangala, N. Fitzkee and D. Zhang, *Langmuir*, 2013, **29**, 10990-10996.
- 23 45. A. Wang, K. Vangala, T. Vo, D. Zhang and N. C. Fitzkee, *J. Phys. Chem. C*, 2014, **118**, 8134-8142.
- 24 46. A. Lopez, F. Lovato, S. Hwan Oh, Y. H. Lai, S. Filbrun, E. A. Driskell and J. D. Driskell, *Talanta*, 2016, **146**, 388-393.
- 25
- 26
- 27 47. S. Hong and X. Li, *J. Nanomater.*, 2013, **2013**, 1-9.
- 28 48. J. K. Yoon, K. Kim and K. S. Shin, *J. Phys. Chem. C*, 2009, **113**, 1769-1774.
- 29 49. W. Jang, H. Byun and J.-H. Kim, *Mater. Chem. Phys.*, 2020, **240**, 122124.
- 30 50. M. Schütz and S. Schlücker, *Phys. Chem. Chem. Phys.*, 2015, **17**, 24356-24360.
- 31 51. T. Horibe, K. Ishii, D. Fukutomi and K. Awazu, *Laser Ther.*, 2015, **24**, 303-310.
- 32 52. R. G. J. Strens and B. J. Wood, *Mineral. Mag.*, 1979, **43**, 347-354.
- 33 53. D. Bartkowiak, V. Merk, V. Reiter-Scherer, U. Gernert, J. P. Rabe, J. Kneipp and E. Kemnitz, *RSC Adv.*, 2016, **6**, 71557-71566.
- 34
- 35 54. M. Iatalese, M. L. Coluccio, V. Onesto, F. Amabo, E. D. Fabrizio and F. Gentile, *Nanoscale Adv.*, 2019, **1**, 228-240.
- 36
- 37
- 38 55. L. Litti and M. Meneghetti, *Phys. Chem. Chem. Phys.*, 2019, **21**, 15515-15522.
- 39 56. B. L. Petros, P. M. Procell, G. H. Campbell and F. H. Collins, *Bulletin of the World Health Organization*, 1989, **67**, 525-533.
- 40
- 41 57. E. R. Tovey and B. A. Baldo, *J. Biochem. Biophys. Methods*, 1989, **19**, 169-183.
- 42 58. D. G. Myszka, T. A. Morton, M. L. Doyle and I. M. Chaiken, *Biophys. Chem.*, 1997, **64**, 127-137.
- 43 59. H. Nygren, M. Werthen and M. Stenberg, *J. Immunol. Methods*, 1987, **101**, 63-71.
- 44 60. P. E. Sheehan and L. J. Whitman, *Nano Lett.*, 2005, **5**, 803-807.
- 45 61. M. Stenberg and H. Nygren, *J. Theor. Biol.*, 1985, **113**, 589-597.
- 46 62. M. A. Penn, D. M. Drake and J. D. Driskell, *Anal. Chem.*, 2013, **85**, 8609-8617.
- 47 63. C. Parolo, A. Sena-Torralba, J. F. Bergua, E. Calucho, C. Fuentes-Chust, L. Hu, L. Rivas, R. Álvarez-Diduk, E. P. Nguyen, S. Cinti, D. Quesada-González and A. Merkoçi, *Nature Protocols*, 2020, **15**, 3788-3816.
- 48
- 49
- 50
- 51 64. S. Dodig, *Biochem. Medica.*, 2009, **19**, 50-62.
- 52 65. X. Liu and Q. Huo, *J. Immunol. Methods*, 2009, **349**, 38-44.
- 53 66. A. Lopez, F. Lovato, S. H. Oh, Y. H. Lai, S. Filbrun, E. A. Driskell and J. D. Driskell, *Talanta*, 2016, **146**, 388-393.
- 54
- 55
- 56
- 57
- 58
- 59
- 60

- 1
2
3 67. J. Deerain, J. Druce, T. Tran, M. Batty, Y. Yoga, M. Fennell, D. E. Dwyer, J. Kok and D. A. Williamson,
4 *J. Clin. Microbiol.*, 2022, **60**, e02479-02421.
5 68. P. de Michelena, I. Torres, Á. Ramos-García, V. Gozalbes, N. Ruiz, A. Sanmartín, P. Botija, S. Poujois,
6 D. Huntley, E. Albert and D. Navarro, *J. Infect.*, 2022, **84**, e64-e66.
7
8
9
10
11
12
13
14
15
16
17
18
19
20
21
22
23
24
25
26
27
28
29
30
31
32
33
34
35
36
37
38
39
40
41
42
43
44
45
46
47
48
49
50
51
52
53
54
55
56
57
58
59
60